



Characterization of Different Rainfall Types from Surface Observations Over a Tropical Location

ANSHUL SISODIYA,¹ SANDEEP PATTNAIK,¹  and HIMADRI BAISYA¹

Abstract—This study characterizes different rainfall types using surface-based instruments (i.e. micro rain radar and laser precipitation monitor) installed at the Indian Institute of Technology Bhubaneswar Jatani, Odisha, India. A total of twelve rainfall cases including four from each season, i.e. pre-monsoon, monsoon and post-monsoon, are considered. The segregation of rainfall is carried out using radar reflectivity and rainfall intensity. In general, initial rainfall is dominantly convective and followed by a stratiform type. Two distinct maxima of radar reflectivity are noted at 3 and 5 km, suggesting the presence of high liquid water content and a melting band. The presence of liquid water content suggests occurrence of a warm rain process with shallow, intense convective cores. Results indicate a higher drop number density below 2 km with smaller size drops for convective rainfall and vice versa for the stratiform rainfall. Furthermore, $Z-R$ relationships are computed for all the cases using a linear regression method, and the results suggest that the stratiform rainfall shows a higher slope parameter and lower intercept parameter as compared to convective rainfall. The distribution of drop number density shows a monomodal and bimodal pattern for convective and stratiform rainfall, respectively.

Key words: Micro rain radar, convective and stratiform rainfall, drop size distribution, $Z-R$ relationship.

1. Introduction

In a climate change scenario, the frequency and magnitude of heavy rainfall events have increased over the Indian region (Goswami et al. 2006; Rajeevan et al. 2008). In addition, there is a significant decreasing trend in the occurrence of long spells of rainfall and increasing trend in frequency of high-

intensity rain (Dash et al. 2009). These heavy rainfall events have posed numerous challenges to the Indian society including flooding, landslides, health hazards, erosion and crop damages. The changing pattern of rainfall is due to changes in dynamical, thermodynamical and microphysical processes responsible for its evolution and growth. Climatologically, three different major rain-making weather systems mainly influence the observation location at IIT Bhubaneswar, Jatani, Khurda, Odisha (region): tropical cyclone landfall (Rao et al. 2019; Wang 2018; Chan 2017), passage of monsoon low-pressure systems (depressions/deep depressions/lows) (Boos et al. 2017; Pottapinjara et al. 2015) and pre-monsoon thundershowers (Narayanan et al. 2016; Hunt et al. 2016). Furthermore, studies have demonstrated multiple physical and dynamical factors influencing convection and rainfall over the study region through passage of monsoon low-pressure systems (MLPS) and pre-monsoon thunderstorms. Recently studies have shown the robust influence of land (surface roughness, topography, moisture and temperature) and cloud microphysical and boundary layer processes on convection and rainfall over the region (Baisya et al. 2017, 2018; Sisodiya et al. 2019; Rai and Pattnaik 2019). Rain drop size distribution (DSD) is an important characteristic of microphysical processes; much of what is known has been determined from different types of observation systems such as Doppler weather radar, micro rain radar (MRR), laser precipitation monitor (LPM) and satellite sensors (Sarkar et al. 2015). However, inferred DSD properties from different instruments are subject to a number of error sources (Wen et al. 2017). Driven by the need for a more accurate measurement of DSD, data from two state-of-the-art observation

Electronic supplementary material The online version of this article (<https://doi.org/10.1007/s00024-019-02338-6>) contains supplementary material, which is available to authorized users.

¹ School of Earth Ocean and Climate Sciences, Indian Institute of Technology Bhubaneswar, Argul, Jatani, Khurda, Odisha 752050, India. E-mail: spt@iitbbs.ac.in

instruments operational over the study location are used in this study. First, MRR, which provides vertical structure of rain up to 6 km for examining the rainfall characteristics aloft, and second is an LPM for rainfall features at the surface. In addition, rainfall data from an automatic weather station (AWS) has been extensively used in this study.

In the Global Atmosphere Research Program's Atlantic Tropical Experiment (GATE) and Convective Precipitation experiment (COPE), very strong bright bands were observed over the tropics, suggesting the presence of stratiform rainfall (Houze 1997; Leon et al. 2016). Furthermore, it was shown that 40% of the precipitation falling on the ocean surface is stratiform in nature (Houze and Cheng 1977; Leary and Houze 1979). In past studies, rain was classified according to the occurrence of bright band and radar reflectivity (Ulbrich and Atlas 2002). The rain classification studies are mostly concentrated on two types of rain, and very few studies focus on the shallow convective or heavy stratiform cases, which occur during transitions between convective to stratiform rain. The existence of melting layers in the radar reflectivity was the sole criterion for classifying it as stratiform, and if there was no indication of the melting layer, the rain was usually regarded as convective (Fabry and Zawadzki 1995). However, in a few cases, the bright band feature is absent in light stratiform rainfall, due to coalescence and orographically forced condensation (Martner et al. 2008; White et al. 2003). Similar classification criteria were used for showing that frequency of occurrence of convective rain is less than 10%, but it contributes more than 50% of total accumulated rain (Rao et al. 2001). Study has showed that the melting layer height varies not only by location but also by topography. The melting layer in a hilly location, such as Shillong, was found between 3 and 4 km (Das and Maitra 2016).

Studies conducted to investigate the variation of vertical profiles of DSD with different rainfall types are very specific to study locations. Few studies found that DSD depends upon micro-scale processes such as break-up mechanism, drop coalescence, evaporation and melting (Das et al. 2010; Peters et al. 2005; Konwar et al. 2014). Previous findings suggested that convective rain is dominated by drop

coalescence and stratiform rain by the drop break-up mechanism and evaporation. One of the aspects of the rain classification is to identify a suitable $Z-R$ relationship for radar meteorology and space applications (Chapon et al. 2008). This widely used method for the measurement of rainfall intensity assumes an exponential relationship of the form $Z = aR^b$, where Z is radar reflectivity, R is rain rate and a and b are constants. The applicability of both these instruments depends on how suitably the $Z-R$ relationship has been derived. After the initial work carried out by Marshall and Palmer (1948), primarily used for the stratiform type of precipitation, various values of a and b have been reported for different regions (Cifelli et al. 2000).

In this context, the current study location, i.e. IIT Bhubaneswar, Jatni, Odisha, India (20.9°N, 85.39°E), has a tropical climate, where maximum rainfall occurs due to passage of monsoon synoptic-scale systems, and pre-monsoon heavy thundershowers provide a unique opportunity to examine the DSD pattern. Furthermore, the state of Odisha is considered a gateway for a majority of MLPS, and the study location is strategically located in the core paths of these MLPS (including lows, depressions and deep depressions). Therefore, the current study is highly relevant in the context of understanding rainfall characteristics of MLPS. The main objective of this study is to not only characterize the rainfall but also to examine the physical processes, parameters and mechanisms associated with it, using ground-based observation systems, i.e. MRR, LPM and AWS, operational over the study location for the 2017 monsoon season. In addition, efforts are made to elucidate some of the unique features of convective and stratiform rainfall.

2. Data and Methodology

2.1. Instruments and Data

Data used for the study are obtained from three instruments, i.e. MRR, an optical laser disdrometer LPM and a rain gauge installed with an AWS, separated by 700 m (Fig. 1).

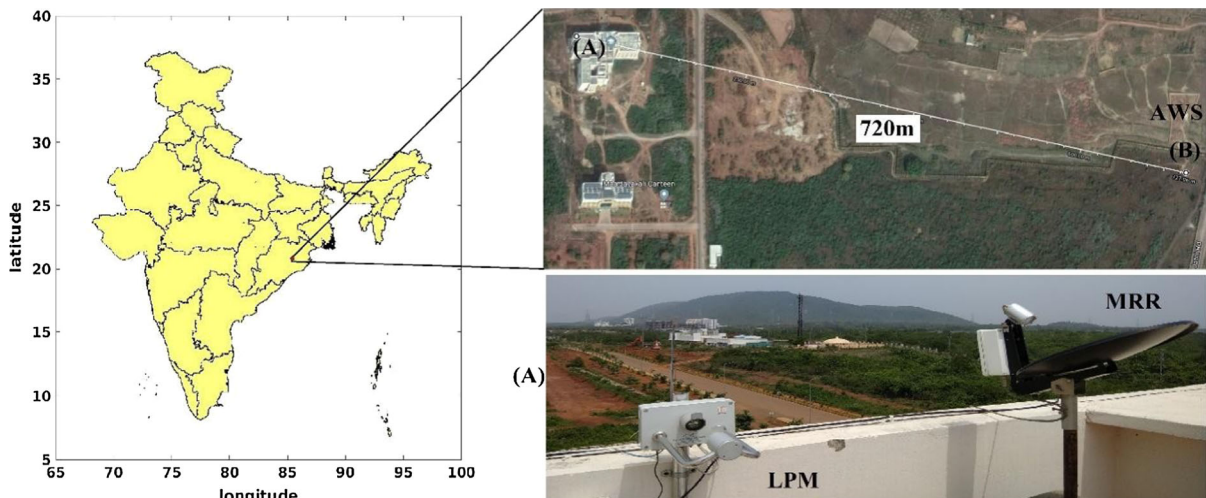


Figure 1 Study location at IIT Bhubaneswar, Argul, Jatni, Odisha, India, detailing the distance using Google Maps

The MRR is a compact 24.1-GHz frequency-modulated-continuous-wave (FM-CW) radar, measuring profiles of DSD, rain rates, liquid water content (LWC) and fall velocity. Due to the high sensitivity and fine temporal resolution, very small amounts of precipitation below the threshold of conventional rain gauges are detectable. At very high frequencies, the quantitatively interpretable height range becomes limited due to attenuation at moderate and higher rain rates (MRR Physics Manual 2011). The details about the MRR specification and temporal scales of data retrieval are shown in Table 1.

The “instantaneous” and “average” reflectivity spectra provided by the online processing are corrected for the noise floor and attenuation. They are displayed in logarithmic scale “dBη”:

$$F(n, i) = 10 \cdot \log \eta(n, i) \tag{1}$$

The Doppler velocity of line n is:

$$v(n) = n \cdot \Delta v = n \Delta f \cdot \lambda / 2 \tag{2}$$

With $\Delta f = 30.52$ -Hz frequency resolution of the Doppler spectra corresponding to the velocity resolution:

$$\Delta v = \Delta f \cdot \lambda / 2 = 0.1905 \text{ ms}^{-1} \tag{3}$$

The radar reflectivity factor obtained from the MRR is defined by:

$$Z = \int_{-\infty}^{\infty} N(D)D^6 dD \tag{4}$$

The LWC is the product of total volume of all the droplets with density of water ρ_w , divided by the scattering volume. It is therefore proportional to the third moment of the DSD

$$\text{LWC} = \rho * \pi/6 \int_{-\infty}^{\infty} N(D)D^3 dD \tag{5}$$

The differential rain rate $rr(D)$ is equal to the volume of the differential droplet number density ($\pi/6 \cdot N(D) \cdot D^3$ multiplied with the terminal falling velocity $v(D)$. From this product, the rain rate is obtained by integration over the drop size:

Table 1

Micro rain radar (MRR) specifications

Frequency	24.1 GHz
Power	50 mW
Operation mode	FM-CW
Beam width	2°
Height resolution	200 m
Temporal resolution	10 s
Number of vertical range gates	30

$$RR = \pi/6 \int_{-\infty}^{\infty} N(D)D^3v(D)dD \quad (6)$$

Another instrument, Thies's LPM, provides parameters, i.e. rainfall intensity, radar reflectivity, precipitable amount, drop number density, with respect to diameter and fall speed of droplets averaged over 1 min. A laser-optical beaming source (laser diode and optics) produces a parallel light beam (infrared, 785 nm, not visible). A photo diode with a lens is situated on the receiver side in order to measure the optical intensity by transforming it into an electrical signal. As the precipitation particle falls through the laser beam (dimension of $22.8 \times 2 \text{ cm}^2$), the receiving signal is reduced. The instrument then computes particle size from the amplitude of reduction, and the fall speed of the particle is determined from the duration of the reduced signal. The measured values are processed by a signal processor and further checked for plausibility. The calculated data are stored for a 1-min interval and then transmitted via the serial interface (Thies CLIMA 2007; Wen et al. 2017).

2.2. Rainfall Classification Criteria

Twelve rain events, four from each of three seasons (i.e. pre-monsoon, monsoon and post-monsoon) are considered in this study for the year 2017 (Table 2). Segregation of rainfall (i.e. stratiform and convective) is carried out based on two criteria, the intensity of rainfall ($> 10 \text{ mm h}^{-1}$) and radar reflectivity ($> 38 \text{ dBZ}$) (Kumar et al. 2011; Badron et al. 2014). In addition, rain rate thresholds are used to classify light, moderate and heavy rainfall, i.e. 0.01–1, 1–10 and 10–100 mm h^{-1} , respectively, to study stratiform and convective rainfall. However, only three cases, one from each season (pre-monsoon, monsoon and post-monsoon), i.e. cases 1, 5 and 9, are discussed in the manuscript, and the remaining case results are presented in the supplementary material.

Based on the India Meteorological Department (IMD) criteria (i.e. a day is considered as rainy day if the daily accumulated rainfall over a station is 2.5 mm) and using the AWS rain gauge data, it is found that there are 76 rainy days in 2017 over the

Table 2

List of cases considered in the study

Case	Dates of event (2017)	Time (IST)	No. of samples (MRR/LPM)	Maximum rain rate (mm h^{-1})
1	6 March	1600–1800	720 ^a	89.71
2	11 March	1800–1900	360 ^a	17.06
3	19 April	1800–2000	720 ^a	27.61
4	27 May	0030–0130	360/60	13.99
5	30 June	1400–1900	1800/300	30.70
6	13 July	1500–2000	1800/300	38.35
7	8 August	0500–0800	1080/180	33.57
8	18 Sept	1100–1600	1800/300	29.43
9	19 October	1300–1800	1800/300	08.20
10	20 October	0400–0800	1440/240	04.77
11	14 1080/180	01.44	November	1800–2100
12	15 1440/240	05.97	November	0700–1100

IST Indian standard time

^aMeans unavailability of data

study location. Of these, 7 days are in pre-monsoon, 57 are in monsoon and 12 days are in post-monsoon season. Furthermore, the cases taken in this study are based on IMD criteria for rather heavy and heavy rainfall events (34.5–64.5 mm for rather heavy rainfall and 64.5–124.4 mm for heavy rainfall) over the location, i.e. IIT Bhubaneswar campus Argul Jatani. For pre-monsoon and post-monsoon seasons, the frequency of rainy days is less, and the cases are considered based on availability of data.

2.3. Synoptic Conditions

The first pre-monsoon isolated thunderstorm case (6 March 2017) was the most intense thunderstorm over the study location, causing 40 mm of rain within 2 h. The recorded maximum wind speed was 22 km h^{-1} at 1640 h and rain started at 1620 h. The occurrence of pre-monsoon thunderstorms is due to combination of multiple factors such as vigorous localized convection (buoyancy) because of intense surface warming, high convective available potential energy (CAPE), and higher moisture availability in the lower to mid-troposphere. The cases considered in pre-monsoon duration are isolated thunderstorms with squall line formation over east and central India (Das 2017). During the second thunderstorm case (i.e.

11 March), the maximum wind speed and accumulated rainfall recorded were 20 km h^{-1} and 10 mm , respectively. The third case considered (i.e. 19 April) had an accumulated rainfall of about 3.5 mm , but the intensity of the wind was strongest, i.e. 35 km hr^{-1} , as compared to other cases. For the fourth case (i.e. 27 May), the maximum speed and rainfall recorded were 20 km h^{-1} and 6.5 mm , respectively. This indicates that these thunderstorms are one of the major reasons for large numbers of deaths due to lightning over this region. As per the Special Relief Commissioner, Odisha, the numbers of deaths were 399 for 2015–2016 and 402 for 2017–2018, hence highlighting the importance of this study.

The monsoon depression cases are synoptic-scale disturbances over the Indian region. The monsoon depressions are weak, warm-core, low-pressure circulation that went through various phases of genesis, intensification and propagation of the storm through extraction of energy from the upper level of the oceans (Sikka 1977). Climatologically, most monsoon depressions that form over the Bay of Bengal propagate toward the Indian land mass through the state of Odisha, and the state is considered as the gateway to MLPS to Indian main land. These synoptic-scale systems are considered as the lifeline for Indian summer monsoon rainfall, therefore making it necessary to understand and quantify their cloud microphysical processes through observation; the study location (i.e. Argul, Jatani) is ideally placed to capture this information. The first case of the monsoon depression was formed over the Saurashtra (28–30 June) and adjoining northeast Arabian Sea and dissipated over Kutch and its neighborhood. This case provided daily accumulated rainfall up to 89 mm over the study location on 30 June between 1430 and 1900 h. The convective behavior of the rain was seen for a very short time initially, followed by light (stratiform) rainfall characteristics. The second case (i.e. 13–18 July) was formed over the Bay of Bengal and moved northwest without further intensification. The system made landfall on the Odisha coast on 18 July. Over the study location, the system contributed heavy rain (50.5 mm) on 13 July 2017 between 1600 and 2000 h. The third monsoon depression (i.e. 8–11 August) was formed over the Bay of Bengal on 8 August, and rainfall was about

64 mm over the study location on the same date. The fourth monsoon depression case (i.e. 18–24 September) formed over northwest Bay of Bengal and neighborhood region and dissipated over Uttar Pradesh and adjoining Uttarakhand. This system contributed about 61.5 mm of rainfall over the study location.

For two post-monsoon cases (i.e. 19 and 20 October), an area of thunderstorm activity was noted by the Joint Typhoon Warning Center (JTWC) as having a partially exposed low-level center over the northern Bay of Bengal. The system was declared a depression by the IMD as it started developing a formative band surrounding a center of deep thunderstorm activity. The system made landfall on 20 October over the Odisha coast near Paradip (80 km from the observation location). Furthermore, during two more post-monsoon cases (14 and 15 November), a low-pressure system formed in the Bay of Bengal, off the southeast coast of India. The system failed to organize further due to strong wind shear and moved northward along the coast. The system later intensified into a depression on 15 November. The lowest pressure observed during the propagation was 1000 hPa with maximum wind speed of 45 km h^{-1} . The system caused heavy rain in some parts of Andhra Pradesh and Odisha, and the study location received 28 mm of rainfall on 15 November 2017 (IMD Monsoon Report 2017, JTWC, and Wikipedia).

3. Results and Discussions

3.1. Validation of MRR and LPM Data with AWS Rain Gauge

Figure 2a, b shows the validation of daily accumulated rainfall data obtained from the LPM and MRR with the AWS rain gauge for the 2017 monsoon. The validation skills are shown in terms of scatter plots, coefficient of correlation and root mean square error (RMSE). The LPM shows better correlation of 0.93 as compared to MRR (0.85). Both these instruments show better correlation for a light rainfall situation; however, the scatter distribution becomes more spread for rainfall greater than 20 mm day^{-1} . Comparison of the LPM and MRR

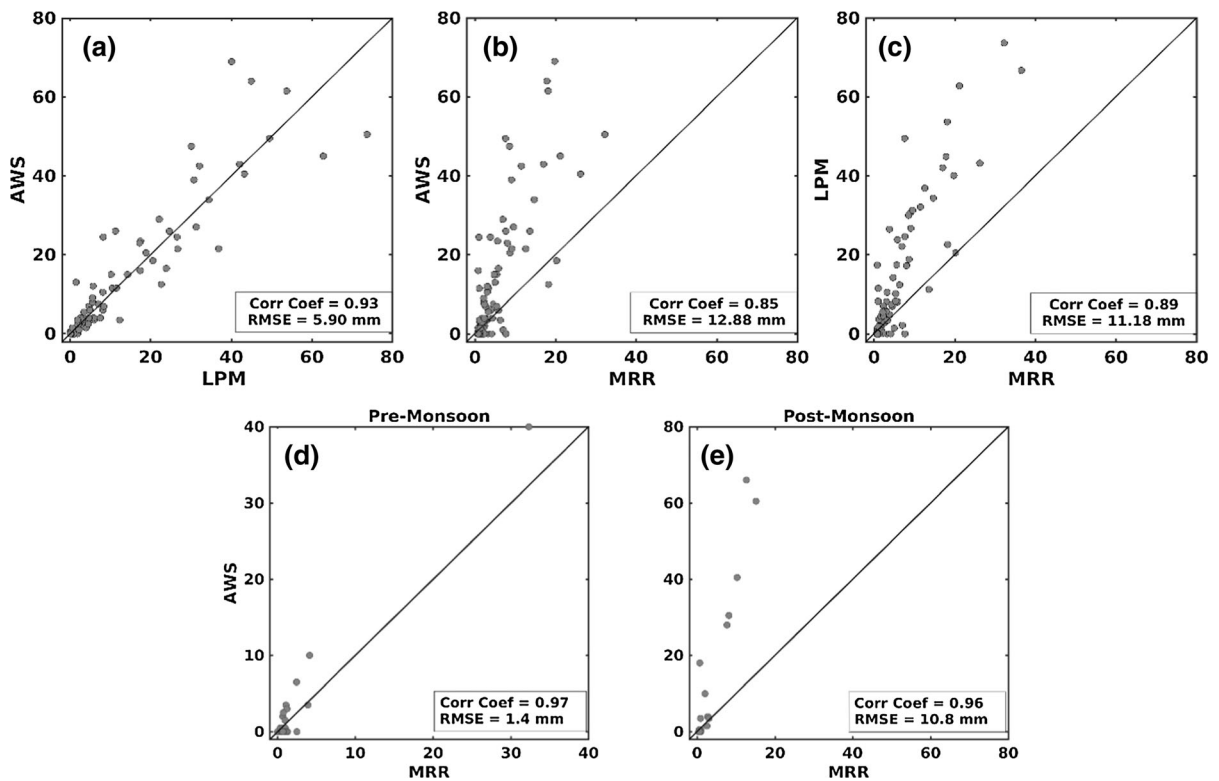


Figure 2

Scatter plot of daily accumulated rainfall from 1 June to 30 September 2017 for three instruments: **a** AWS and LPM, **b** AWS and MRR, **c** LPM and MRR, **d** AWS and MRR for pre-monsoon season and **e** AWS and MRR for post-monsoon season

(Fig. 2c) suggest that rainfall is underestimated by the MRR at 200 m, which may be due to the instrument's inability to capture small rain drops and attenuation in moderate and higher rain rates. Total rain recorded over the study location during the 2017 monsoon season by the AWS and LPM is 1258 mm and 1209.6 mm, respectively. It is found that convective rain occurs 7.97% of the time, whereas stratiform rain occurs about 92.03% of the time. The relative contribution to the total accumulated rain during the season from convective rainfall was 74% (895.1 mm), suggesting convective rainfall has a large contribution toward overall monsoon seasonal rainfall.

3.2. Segregation of Rainfall Type and Associated Parameters

MRR altitude time series data of radar reflectivity and rain rate for three cases from each phase are

presented in Fig. 3a–f. In general, it is found that intense convective rain (reflectivity > 38 dBZ, surface rain rate > 10 mm h⁻¹) occurred for about 1–2 h for all cases except for the post-monsoon case 9 (Fig. 3 a, c). A stronger evolution of melting zones (stratiform type) is noted at about 4–6 km, following the intense convective rainfall. This indicates that during intense rainfall hours, there is strong attenuation of radar signals, causing loss of data at upper-level heights (Fig. 3b). For deep convective thunderclouds, the higher radar reflectivity values are found near the surface along with a higher rate of fall speed of hydrometeors. Furthermore, the attenuation is also higher for deep convective clouds owing to the absence of a melting layer (as seen in case 1 above 2–3 km). Similarly, shallow convective cells also show similar radar reflectivity profiles closer to the surface, except for the absence of a signature of rain drops at upper levels. However, the stratiform rainfall is associated with the weakening of the deep

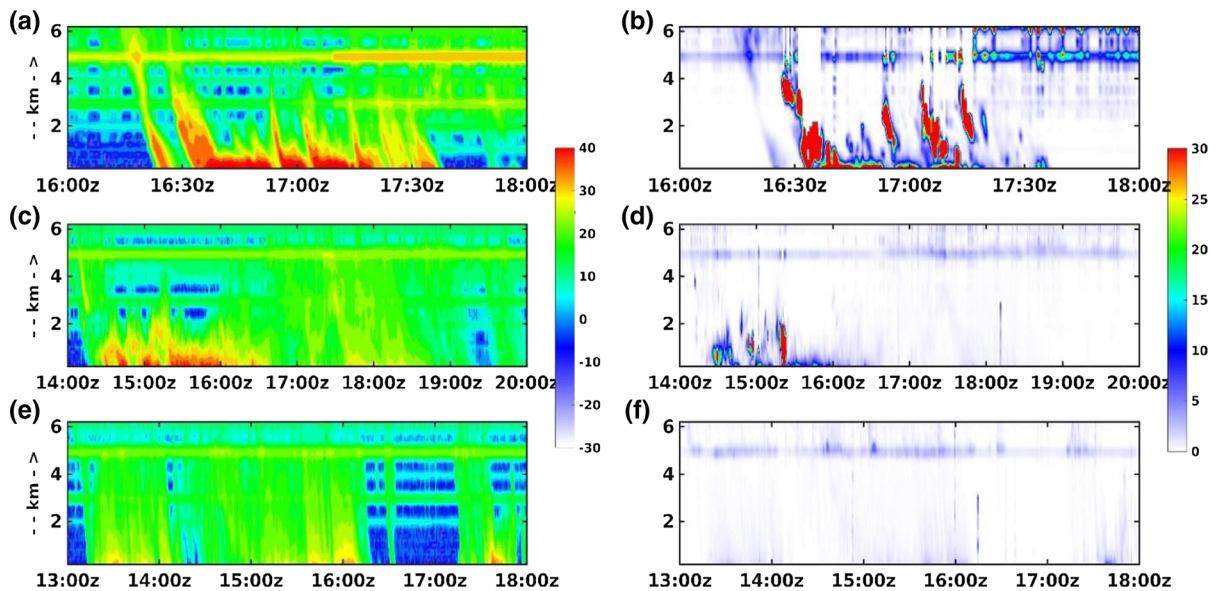


Figure 3

Vertical profiles of radar reflectivity (dbZ) and rain rate (mm h^{-1}) on respective dates. **a, b** Case 1 (6 March 2017, 1600–1800 h IST). **c, d** Case 5 (30 June 2017, 1400–2000 h). **e–f** Case 3 (19 October 2017, 1300–1800 h)

convection. As the surface convection weakens, the vertical updraft decreases and water vapor tends to raise up to the melting layer. As the intensity of convective rain decreases, the profile starts to show the signature of a melting layer above the surface (due to less attenuation, the capability of MRR to capture the melting layer increases) considered as stratiform rainfall. The vertical profile of stratiform rain shows a high peak near the melting zone and shows a very uniform structure of the rain profile below the bright band (unlike the convective rain with high radar reflectivity near the surface). It is evident in all three cases that the rain initiated as convective and was followed by the stratiform type with a rate less than 10 mm h^{-1} ; however, for case 9, the whole event was dominated by stratiform signatures (Fig. 1 e, f). These results suggest that for the pre-monsoon and monsoon cases, shallow convective cells are responsible for high-intensity rainfall during the initial hours followed by a stratiform component.

Now, MRR rainfall intensity at 200 m is classified into three classes: (1) $0.01\text{--}1 \text{ mm h}^{-1}$ (black lines), (2) $1\text{--}10 \text{ mm h}^{-1}$ (blue line), (3) $10\text{--}100 \text{ mm h}^{-1}$ (red line) for low and intense rainfall types. Mean profiles of radar reflectivity for different rain rate

classes for all cases are shown in Fig. 4a–l. Results suggest the presence of a melting layer signature at about 5 km for all rain rate classes in all cases, during stratiform as well as convective type of rainfall (Fig. 4 a, e, i). This indicates that in case 9, the discussions are limited only to stratiform rainfall, as intense rainfall (i.e. $10\text{--}100 \text{ mm h}^{-1}$) was absent for this case. The first rainfall types are segregated in terms of their aforementioned intensities. Then, based on time of occurrence of respective rainfall types, their time-averaged profiles of associated parameters (i.e. radar reflectivity, rain rate, fall velocity and LWC) are shown in Fig. 4.

In general, it is found that there are two distinct radar reflectivity maximums at 3 and 5 km for all rainfall thresholds, suggesting the presence of large liquid water and a melting band over the region. Furthermore, this indicates that even at higher thresholds of rainfall, i.e. $10\text{--}100 \text{ mm h}^{-1}$, rainfall type is not purely convective in nature. It is seen that the maximum negative gradient of radar reflectivity (about 20 dbZ km^{-1}) closer to the surface corresponds to a sudden increasing in rain rate and LWC, suggesting the presence of shallow convective cells within 2-km height from the surface (Fig. 4 e–g, S5).

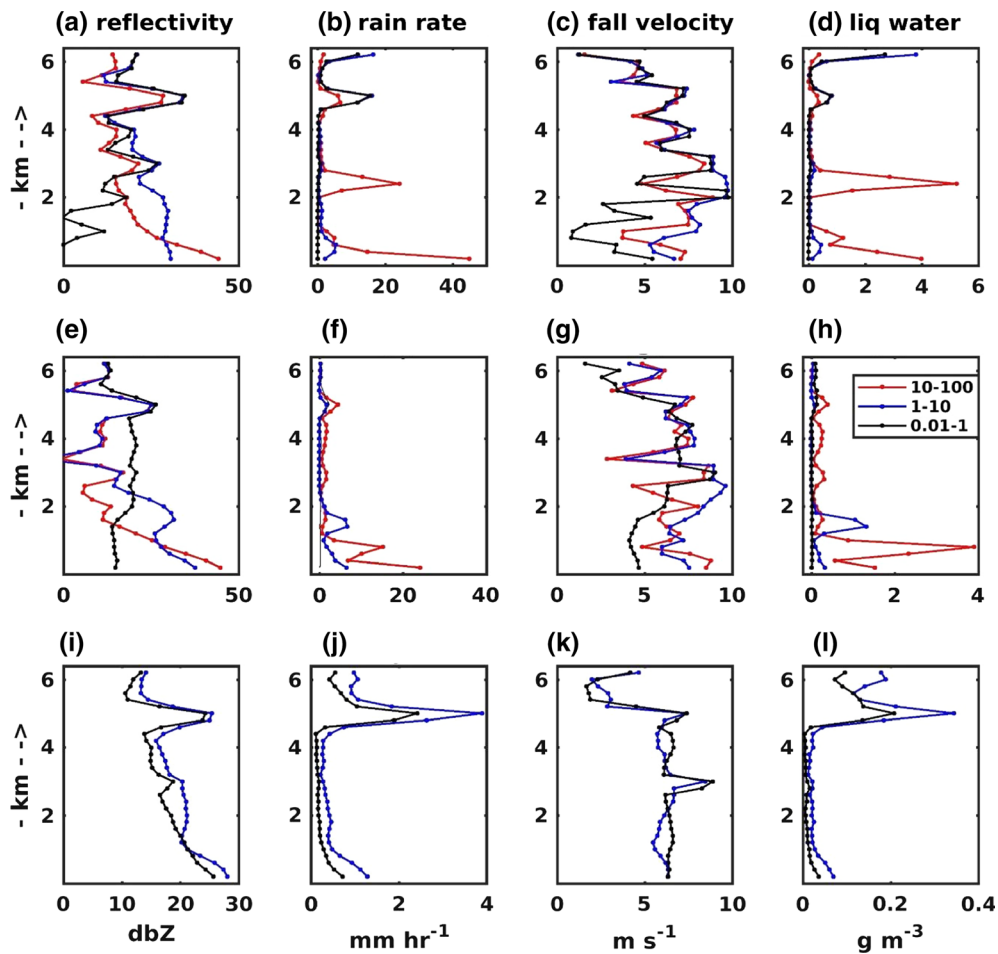


Figure 4

Time-averaged vertical profiles of (a, e, i) radar reflectivity (dbZ), (b, f, j) rain rate (mm h^{-1}), (c, g, k) fall velocity (m s^{-1}) and (d, h, l) LWC (g m^{-3}) for three cases. a–d Case 1 (6 March 2017), e–h case 5 (30 June 2017) and i–l case 9 (19 October 2017). Rain is classified into three categories as (1) $0.01\text{--}1 \text{ mm h}^{-1}$ (black line), (2) $1\text{--}10 \text{ mm h}^{-1}$ (blue line) and (3) $10\text{--}100 \text{ mm h}^{-1}$ (red line)

LWC profiles (Fig. 4 c, g, k) show a coherent pattern with rain rate profiles for all cases. For low and moderate rainfall, the value of LWC appears to be very small (i.e. $0\text{--}1 \text{ g m}^{-3}$) and does not vary much with height. However, interestingly large variations are seen for intense and moderate rainfall (i.e. $10\text{--}100 \text{ mm h}^{-1}$ and $1\text{--}10 \text{ mm h}^{-1}$) closer to the surface, where sudden peaks (i.e. up to 10 g m^{-3}) are noted below 2 km, suggesting a warm rain formation (with higher LWC).

The fall velocity profile show a steep negative gradient above melting layer height ($> 5 \text{ km}$) in all rain types, indicating the presence of slow-moving, downward, frozen hydrometeors (Fig. 4 c, g, k). It is

noted that fall velocities have higher magnitudes ($> 5 \text{ m s}^{-1}$) for all intense rainfall threshold cases, except for case 1 and case 3, which have low- and moderate-intensity rainfall thresholds, respectively, and have significantly less fall speed ($< 2 \text{ m s}^{-1}$). This suggests that these particular rainfall thresholds have small drop sizes particularly closer to the surface. This point is further elaborated in the next section. It is also noted that for most of the rainfall types, there is a peak at 3 km for fall speed, suggesting an increase in LWC in that zone.

3.3. Drop Size Distribution (DSD)

In addition to the characterization of rain types and associated parameters, it is also necessary to understand the mechanism behind the evolution of these precipitating systems. In Fig. 5a–e, time-averaged vertical profiles of drop number density (N) are plotted with respect to drop size (D) in logarithmic scale for both types of rain (i.e. stratiform and convective) based on radar reflectivity threshold (> 38 dbZ) and rainfall (> 10 mm h⁻¹). Averaged DSD profiles are for the specific time periods based on aforementioned criteria and valid only in rain regions, i.e. below the zero-degree isotherm (about 5 km) and right of the dashed lines, as the MRR discards data for lesser diameter bins due to quality control.

For stratiform cases, a positive slope of number density indicates the breakup of bigger drops into smaller drops (Fig. 5 b, d, f). The number density starts decreasing ($dN/dz > 0$) for smaller-diameter bins suggesting a drop breakup mechanism prevalent during stratiform rain. In all three cases of convective rain, the number density shows negative gradients

with respect to drop size diameter below 3 km (Fig. 5a, c). Results clearly suggest that for convective rainfall, drop number density increases with decrease in height showing negative slope ($dD/dz < 0$ and $dN/dz < 0$) leading to very high drop number density below 2 km with small size drops. It also indicates the presence of shallow convective cores near the surface with dominance of a drop coalescence process leading to increase in drop number density; this feature is absent in case of stratiform rainfall. Above 2 km, drop number density remains the same as shown by the gradual slope of profiles suggesting the domain processes such as evaporation, drop breakup and drop coalescence are equally dominating, hence canceling out the net effect on drop size growth (Fig. 3a, c, e).

3.4. Z–R Relationship

In this section, coefficients of the Z–R relationship are computed using linear regression analysis. First, the Z–R relationship is computed separately for convective and stratiform rainfall, but the variations

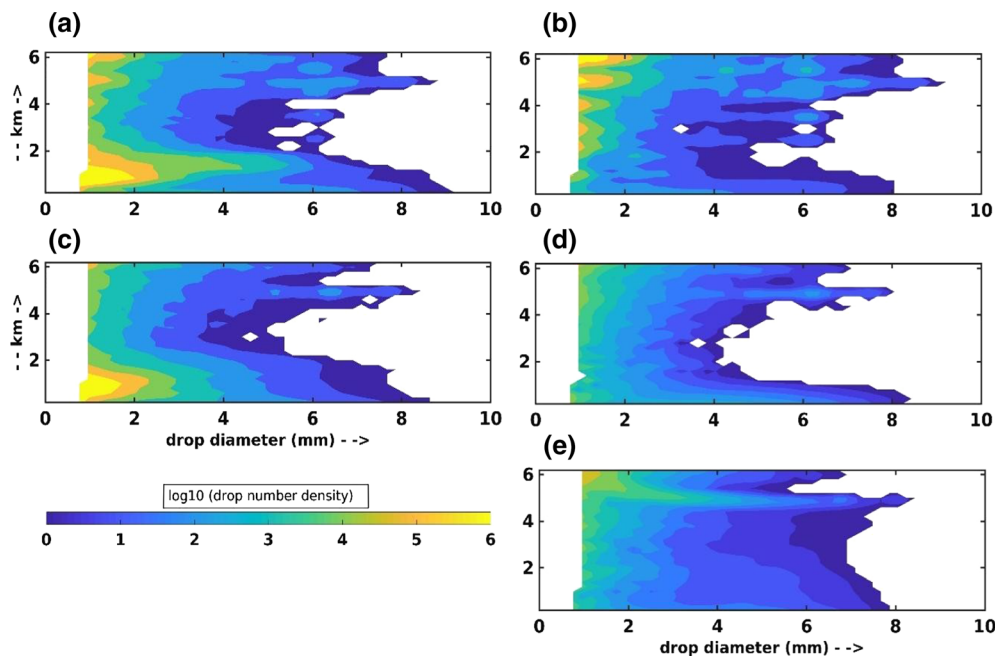


Figure 5

Vertical profiles (time-averaged) of \log_{10} of drop number density (N) for three rainfall events: **a, b** case 1 (6 March 2017); **c, d** case 2 (30 June 2017); **e** case 3 (19 October 2017)

in intercept parameter ‘ a ’ were large in convective cases, which does not help select a single relationship for all convective cases. Thus, a single relationship is preferred over segregated rainfall. It is found that as the rain rate over surface increases, the intercept parameter increases while slope parameter ‘ b ’ decreases. Stratiform rainfall shows a higher slope parameter and lower intercept parameter as compared to convective rainfall. Table 3 shows the values of slope and intercept parameters along with a coefficient of determination for all cases considered in this study.

The relationships for pre-, post- and monsoon season are computed, and the results show similar patterns for both instruments (Fig. 6a–f). Intercept ‘ a ’ and slope parameter ‘ b ’ show higher and lower values, respectively, for intense pre-monsoon episodes, whereas as the rain intensity is reduced (mostly in post-monsoon cases), values of slope and intercept parameters are reversed in their magnitudes.

3.5. Rain Characteristics Over Surface

Drop number density snapshots for 1-min intervals from the LPM are shown in in Fig. 7a–e with respect to the diameter of drop particles (mm) and drop fall velocity for the last three cases, respectively. It is found that convective rains contain the highest number for smaller drop sizes (< 1 mm), whereas stratiform rain drop particle size varies from smaller to moderate drop sizes up to 3 mm. The drop number

density distribution with respect to drop sizes follow a mono-modal and bimodal pattern for convective and stratiform rain types, respectively. Furthermore, the number of drops are lesser in stratiform rain compared to convective rain. Results suggest that closer to the surface, convective rain is associated with a large number of drops with a maximum number of smaller drop size bins, and stratiform rain is associated with larger rain drops with a lesser number density.

4. Conclusions

The segregation of rainfall with possible micro-physical properties of different types of rainfall-bearing systems (twelve cases) are examined from MRR and LPM observation data sets over a tropical station, i.e. IIT Bhubaneswar, Jatani, Khurda Odisha, India (85.7°E, 20.17°N). The study location is at the eastern coast of India, which is a pathway to MLPS, and post-monsoon cyclonic storms also impacted by pre-monsoon thundershowers. The rainfall segregations are based on radar reflectivity and intensity of rainfall. Validation of MRR and LPM with the AWS rain gauge over the location is in close agreement for moderate rainfall, but variations are noted for accumulated rain greater than 20 mm day⁻¹. In general, it is found that the rain-bearing systems have both convective as well as stratiform rain type signatures. However, it is noted that initial phases of the rainfall are convective in nature and are followed by stratiform rainfall. The bright band is found at about 5 km for low and intensified rainfall; therefore, segregating rainfall into convective or stratiform type purely based on presence of the bright band is not appropriate. By analyzing vertical profiles of the rain rate and associated parameters, it is imminent that shallow but intense convective cores are dominant below 2-km height, which are mainly responsible for intense rainfall for these events. Examining vertical profiles of DSD, it is found that convective rain is dominated by the drop coalescence process with high-diameter drop size as compared to stratiform rain, where the drop breakup mechanism dominates, leading to smaller rain drops close to the surface. Over the surface, drop number density distribution clearly

Table 3

Z–R relationship computed for the cases in the study for both instruments

S. No.	Cases	MRR	R2	LPM	R2
1	Pre-monsoon 1	$Z = 470R^{1.17}$	0.97	–	–
2	Pre-monsoon 2	$Z = 395R^{1.36}$	0.93	–	–
3	Pre-monsoon 3	$Z = 406R^{1.24}$	0.87	–	–
4	Pre-monsoon 4	$Z = 470R^{1.26}$	0.89	$Z = 264R^{1.37}$	0.95
5	Monsoon 1	$Z = 414R^{1.23}$	0.94	$Z = 330R^{1.33}$	0.96
6	Monsoon 2	$Z = 369R^{1.35}$	0.90	$Z = 335R^{1.37}$	0.97
7	Monsoon 3	$Z = 346R^{1.29}$	0.93	$Z = 271R^{1.38}$	0.98
8	Monsoon 4	$Z = 388R^{1.30}$	0.88	$Z = 383R^{1.23}$	0.93
9	Post-monsoon 1	$Z = 362R^{1.32}$	0.87	$Z = 267R^{1.33}$	0.95
10	Post-monsoon 2	$Z = 245R^{1.43}$	0.89	$Z = 112R^{1.43}$	0.89
11	Post-monsoon 3	$Z = 326R^{1.26}$	0.84	$Z = 298R^{1.41}$	0.97
12	Post-monsoon 4	$Z = 306R^{1.31}$	0.95	$Z = 217R^{1.41}$	0.94

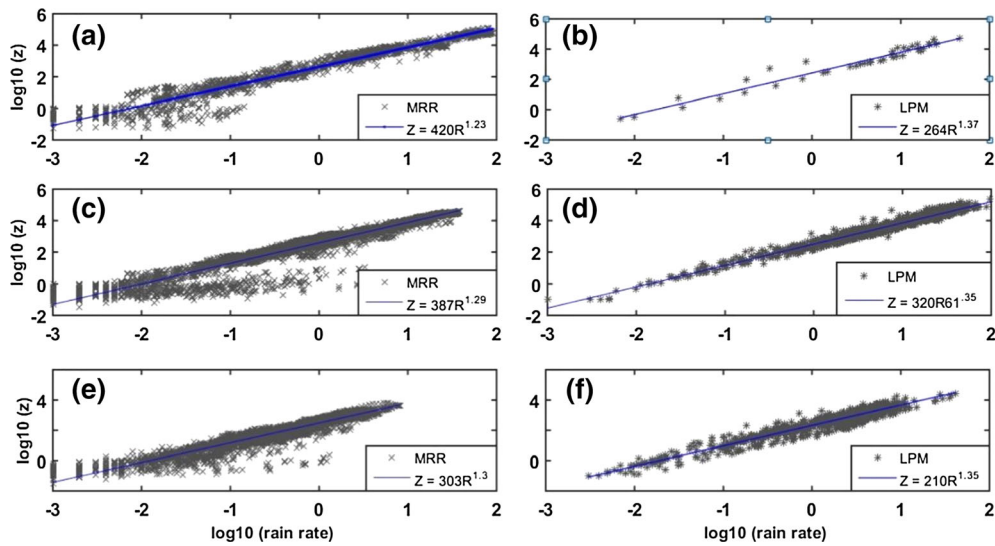


Figure 6

Scatter plot for $\log_{10}(Z) - \log_{10}(RR)$ relationship obtained by linear regression method for both instrument: (a, c, e) for MRR and (b, d, f) for LPM for pre-monsoon, monsoon and post-monsoon cases, respectively

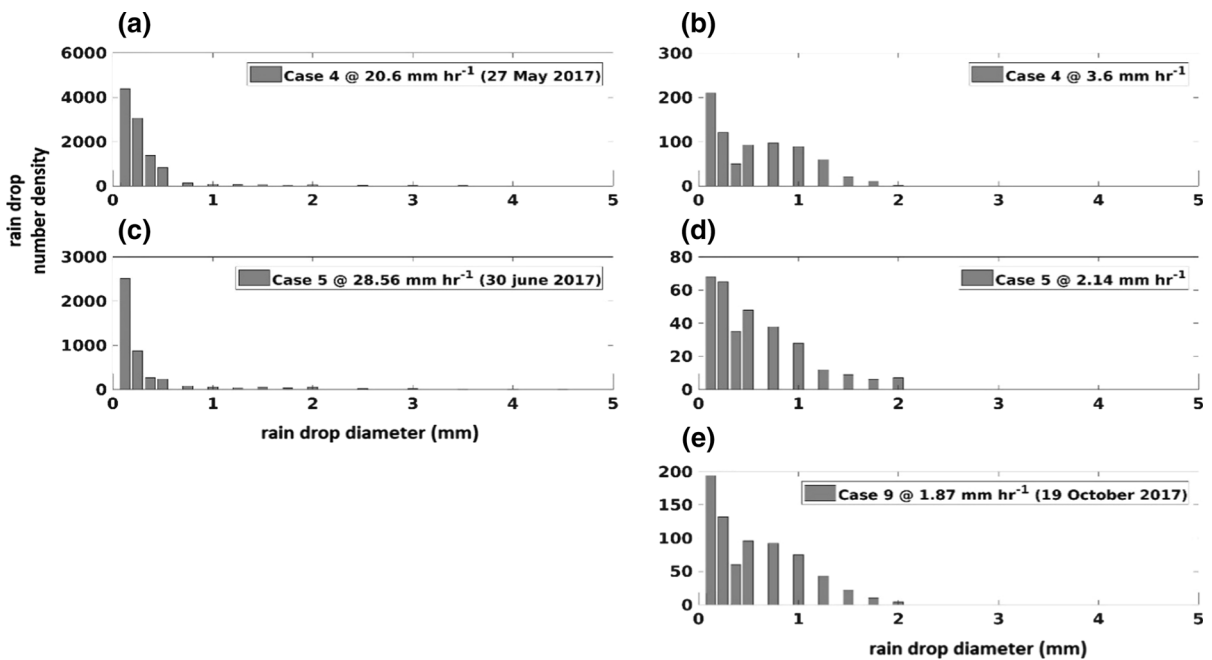


Figure 7

Drop number distribution at surface from the LPM for the three cases: a, b for case 4 (27 May 2017); c, d case 5 (30 June 2017); and e case 9 (19 October 2017) segregated based on convective and stratiform rainfall

shows a bimodal and mono-modal distribution for stratiform and convective rainfall, respectively. It should be mentioned that the results of three cases (in

three different seasons) are extensively discussed in this manuscript, and, in order to avoid redundancy, the results of the remaining nine cases are presented

in the supplementary materials (S1–S9). This confirms that the results of remaining nine cases presented in the supplementary have similar characteristics as that of these three cases discussed, and the scientific inferences drawn in this paper are based on all 12 cases considered. The findings of the study are of high relevance considering the strategic location of observations, i.e. in the core pathway of a majority of MLPS having genesis over the Bay of Bengal. This new information will be highly valuable to accurately quantify and characterize the representation of different rainfall types in the numerical models for better prediction and a better understanding of cloud processes. This knowledge will also facilitate operational agencies for accurate prediction of location-specific thunderstorm and lightning events over the region with adequate lead time to prevent loss of lives and property.

Acknowledgements

The authors would like to thank the Indian Institute of Technology Bhubaneswar (grant no. A16ES09006) for providing research facilities and helpful assistance required for this purpose. Furthermore, our gratitude is extended to the funding agencies, namely the Ministry of Earth Sciences (MoES), India (RP-083), Department of Science and Technology (DST), India (RP-132), and Scientific and Engineering Board (SERB), India (RP-193), for their support to carry out this research.

Publisher's Note Springer Nature remains neutral with regard to jurisdictional claims in published maps and institutional affiliations.

REFERENCES

- Badron, K., Ismail, A. F., Asnawi, A. L., Malik, N. F. A., Abidin, S. Z., & Dzulkifly, S. (2014). Classification of precipitation types detected in Malaysia. *International Journal of Electrical, Electronic and Communication Sciences*, 8(8), 1379–1383.
- Baisya, H., Pattnaik, S., Hazra, V., Sisodiya, A., & Rai, D. (2018). Ramifications of atmospheric humidity on monsoon depressions over the Indian subcontinent. *Scientific Reports*, 8, 9927. <https://doi.org/10.1038/s41598-018-28365-2>.
- Baisya, H., Pattnaik, S., & Rajesh, P. V. (2017). Land surface-precipitation feedback analysis for a landfalling monsoon depression in the Indian region. *Journal of Advances in Modeling Earth Systems*, 9(1), 712–726.
- Boos, W. R., Mapes, B. E., & Murthy, V. S. (2017). Chapter 15: Potential vorticity structure and propagation mechanism of Indian monsoon depressions. In *The global monsoon system. World scientific series on Asia-Pacific weather and climate* (Vol. 9, pp. 187–199). https://doi.org/10.1142/9789813200913_0015.
- Chan, J. C. L. (2017). Physical mechanisms responsible for Track Changes and Rainfall Distribution Associated with Tropical Cyclone Landfall. <https://doi.org/10.1093/oxfordhb/9780190699420.013.16>.
- Chapon, B., Delrieu, G., Gosset, M., & Boudevillain, B. (2008). Variability of rain drop size distribution and its effect on the Z–R relationship: A case study for intense Mediterranean rainfall. *Atmospheric Research*, 87(1), 52–65.
- Cifelli, R., Williams, C. R., Rajopadhyaya, D. K., Avery, S. K., Gage, K. S., & May, P. T. (2000). Drop-size distribution characteristics in tropical mesoscale convective systems. *Journal of Applied Meteorology*, 39(6), 760–777.
- Das, S. (2017). Severe thunderstorm observation and modeling—a review. *Vayu Mandal*, 43(2), 1–29.
- Das, S., & Maitra, A. (2016). Vertical profile of rain: Ka band radar observations at tropical locations. *Journal of Hydrology*, 534, 31–41.
- Das, S., Shukla, A. K., & Maitra, A. (2010). Investigation of vertical profile of rain microstructure at Ahmedabad in Indian tropical region. *Advances in Space Research*, 45, 1235–1243.
- Dash, S. K., Kulkarni, M. A., Mohanty, U. C., & Prasad, K. (2009). Changes in the characteristics of rain events in India. *Journal of Geophysical Research: Atmosphere*, 114(D10109), 1–12.
- Fabry, F., & Zawadzki, I. (1995). Long-term radar observations of the melting layer of precipitation and their interpretation. *Journal of the Atmospheric Science*, 52, 838–851.
- Goswami, B. N., Venugopal, V., Sengupta, D., Madhusoodanan, M. S., & Xavier, P. K. (2006). Increasing trend of extreme rain events in a warming environment. *Science*, 314, 1442–1445.
- Houze, R. A. (1997). Stratiform precipitation in regions of convection: A meteorological paradox? *Bulletin of American Meteorological Society*, 78, 2179–2196.
- Houze, R. A., & Cheng, C. P. (1977). Radar characteristics of tropical convection observed during GATE: Mean properties and trends over the summer season. *Monthly Weather Review*, 105, 964–980.
- Hunt, K. M. R., Turner, A. G., Inness, P. M., Parker, D. E., & Levine, R. C. (2016). On the structure and dynamics of Indian Monsoon Depressions. *Monthly Weather Review*, 144, 3391–3416.
- Konwar, M., Das, S. K., Deshpande, S. M., Chakravarty, K., & Goswami, B. N. (2014). Microphysics of clouds and rain over the Western Ghat. *Journal of Geophysical Research: Atmosphere*, 119, 6140–6159.
- Kumar, L. S., Lee, Y. H., Yeo, J. X., & Ong, J. T. (2011). Tropical rain classification and estimation of rain from Z–R (reflectivity–rain rate) relationships. *Progress in Electromagnetics Research B*, 32, 107–127.

- Leary, C. A., & Houze, R. A. (1979). The structure and evolution of convection in a tropical cloud cluster. *Journal of the Atmospheric Science*, 36, 437–457.
- Leon, D. C., French, J. R., Lasher-Trapp, S., Blyth, A. M., et al. (2016). The Convective Precipitation Experiment (COPE): Investigating the origins of heavy precipitation in the southwestern United Kingdom. *Bulletin of the American Meteorological Society*, 97, 1003–1020.
- Marshall, J. S., & Palmer, W. M. K. (1948). The distribution of raindrops with size. *Journal of Meteorology*, 5, 165–166.
- Martner, B. E., Yuter, S. E., White, A. B., Matrosov, S. Y., Kingsmill, D. E., & Ralph, D. E. (2008). Raindrop size distributions and rain characteristics in California coastal rainfall for periods with and without a radar bright band. *Journal of Hydrometeorology*, 9, 408–425.
- METEK Micro Rain Radar. (2011). Physics Manual, Valid for MRR Service Version 6.0.0.2S.
- Narayanan, S., Vishwanathan, G., & Mrudula, G. (2016). Possible development mechanisms of pre-monsoon thunderstorms over northeast and east India. In *Proceedings SPIE 9882, Remote Sensing and Modeling of the Atmosphere, Oceans, and Interactions VI*, 98821U.
- Peters, G., Fischer, B., Münster, H., Clemens, M., & Wagner, A. (2005). Profiles of raindrop size distributions as retrieved by micro rain radars. *Journal of Applied Meteorology and Climatology*, 44, 1930–1949.
- Pottapinjara, V., Girishkumar, M. S., Sivareddy, S., Ravichandran, M., & Murtugudde, R. (2015). Relation between the upper ocean heat content in the equatorial Atlantic during boreal spring and the Indian monsoon rainfall during June–September. *International Journal of Climatology*, 36(6), 2469–2480.
- Rai, D., & Pattnaik, S. (2019). Evaluation of WRF planetary boundary layer parameterization schemes for simulation of monsoon depressions over India. *Meteorology and Atmospheric Physics*, 131(5), 1529–1548.
- Rajeevan, M., Bhate, J., & Jaswal, A. K. (2008). Analysis of variability and trends of extreme rainfall events over India using 104 years of gridded daily rainfall data. *Geophysical Research Letters*, 35, 1–6.
- Rao, T. N., Rao, T. N., Mohan, K., & Raghavan, S. (2001). Classification of tropical precipitating systems and associated Z–R relationships. *Journal of Geophysical Research: Atmosphere*, 106, 17699–17711.
- Rao, N. N., Rao, V. B., Ramakrishna, S. S., & Rao, B. S. (2019). Moisture budget of the tropical cyclones formed over the Bay of Bengal: Role of soil moisture after landfall. *Pure and Applied Geophysics*, 176, 441–461.
- Sarkar, T., Das, S., & Maitra, A. (2015). Assessment of different raindrop size measuring techniques: Intercomparison of Doppler radar, impact and optical disdrometer. *Atmospheric Research*, 160, 15–27.
- Sikka, D. R. (1977). Some aspects of the life history, structure and movement of monsoon depressions. *Pure and Applied Geophysics*, 115, 1501–1529.
- Sisodiya, A., Pattnaik, S., Baisya, H., Bhat, G. S., & Turner, A. G. (2019). Simulation of location specific severe thunderstorm events using high resolution land assimilation”. *Dynamics of Atmospheres and Oceans*. <https://doi.org/10.1016/j.dynatmoce.2019.101098>.
- Thies CLIMA, (2007). Instructions for Use, Laser Precipitation Monitor 5.4110.xx.x00 V2.5x STD. *Thies Technology Report*.
- Ulbrich, C. W., & Atlas, D. (2002). On the separation of tropical convective and stratiform rains. *Journal of Applied Meteorology and Climatology*, 41, 188–195.
- Wang, Z. (2018). What is the key features of convection leading up to tropical cyclone formation. *Journal of the Atmospheric Sciences*, 75, 1609–1629. (**Oxford Handbooks Online**).
- Wen, L., Zhao, K., Zhang, G., Liu, S., & Chen, G. (2017). Impact of instrument on estimated raindrops size distribution, radar parameters, and model microphysics during Mei-Yu season in East China. *Journal of Atmospheric and Oceanic Technology*, 43(5), 1021–1037.
- White, A. B., Neiman, P. J., Ralph, F. M., Kingsmill, D. E., Persson, P. O. G., & Olume, V. (2003). Coastal orographic rainfall processes observed by radar during the California land-falling jets experiment. *Journal of Hydrometeorology*, 4, 264–282.